RSC Advances

PAPER

View Article Online
View Journal | View Issue

Cite this: *RSC Adv.*, 2018, **8**, 31296

Flexible solid-state supercapacitor based on tin oxide/reduced graphene oxide/bacterial nanocellulose†

Keng-Ku Liu,[a] Qisheng Jiang,[a] Clayton Kacica,[b] Hamed Gholami Derami,[a] Pratim Biswas *[b] and Srikanth Singamaneni *[a]

We demonstrate a flexible and light-weight supercapacitor based on bacterial nanocellulose (BNC) incorporated with tin oxide (SnO_2) nanoparticles, graphene oxide (GO) and poly(3,4-ethylenedioxyiophene)-poly(styrenesulfonate) (PEDOT:PSS). The SnO_2 and GO flakes are introduced into the fibrous nanocellulose matrix during bacteria-mediated synthesis. The flexible PEDOT:PSS/SnO_2/rGO/BNC electrodes exhibited excellent electrochemical performance with a capacitance of 445 F g^{-1} at 2 A g^{-1} and outstanding cycling stability with 84.1% capacitance retention over 2500 charge/discharge cycles. The flexible solid-state supercapacitors fabricated using PEDOT:PSS/SnO_2/rGO/BNC electrodes and poly(vinyl alcohol) (PVA)-H_2SO_4 coated BNC as a separator exhibited excellent energy storage performance. The fabrication method demonstrated here is highly scalable and opens up new opportunities for the fabrication of flexible cellulose-based energy storage devices.

Received 20th June 2018
Accepted 23rd August 2018

DOI: 10.1039/c8ra05270k

rsc.li/rsc-advances

1. Introduction

Flexible energy storage devices are extremely important for a wide range of flexible and wearable electronic and optoelectronic devices that are finding numerous applications in healthcare and consumer electronics.[1–4] Supercapacitors have attracted extensive attention as flexible energy storage devices due to their higher power density, rapid charge–discharge characteristics, and long cycle life.[5,6] Owing to their high surface area, high electrical conductivity and superior stability, carbon-based materials such as carbon nanotubes (CNT), carbon nanofibers (CNF), graphene, graphene oxide (GO) and activated carbon are widely employed in electric double-layer capacitors (EDLCs).[3,5,7–13] Pseudocapacitive materials (*e.g.* conducting polymers and metal oxides) are commonly integrated with EDLCs to form hybrid supercapacitors with enhanced capacitance and energy densities owing to the fast and highly-reversible faradic processes between the electroactive species on the surface of the electrode and the electrolyte.[6,14–19] Among the metal oxides, tin oxide (SnO_2) has attracted much attention due to its high theoretical capacity (~782 mA h g^{-1}), high abundance and low cost.[20–23]

Cellulosic materials are considered to be highly promising for flexible electrical energy storage devices due to their flexibility, highly porous structure, lightweight, and low cost.[14,24–30] It has been demonstrated that a composite structure comprised of cellulose paper and carbon materials exhibited promising energy-storage performance.[7,8,25,30] Recently, Ko and co-workers have reported flexible supercapacitor electrodes composed of metal and pseudocapacitive nanoparticles on a metal-like paper, which significantly increases the areal capacitance and rate capability.[24] Chen *et al.* have demonstrated an all-wood-structured supercapacitor, which exhibited high energy storage capacity.[31] The components of this all-wood-structured supercapacitor are biocompatible, environmentally friendly, and low-cost.[31] More recently, we have demonstrated an *in situ* formation of GO/bacterial nanocellulose (BNC) composite as light-weight supercapacitor electrode.[32] Additionally, this GO/BNC-based supercapacitor exhibited excellent energy storage properties and stability.[32] These recent reports further signify the advantages of cellulose for the applications in energy storage. However, compared to hybrid supercapacitors, EDLCs exhibit relative low specific capacitance. Thus, the combination of cellulosic materials-based EDLCs with pseudocapacitive materials to form hybrid supercapacitors is considered to be highly promising for flexible energy storage devices with enhanced energy storage performance.

In this work, we demonstrate the incorporation of SnO_2 and GO flakes into nanofibrous cellulose matrix during its bacteria-mediated growth followed by coating with a conductive polymer, poly(3,4-ethylenedioxyiophene)-poly(styrenesulfonate) (PEDOT:PSS), to realize a flexible, light-weight, and solid-state

[a]*Department of Mechanical Engineering and Materials Science, Institute of Materials Science and Engineering, Washington University in St. Louis, St Louis, Missouri 63130, USA. E-mail: singamaneni@wustl.edu*

[b]*Department of Energy, Environmental and Chemical Engineering, Washington University in St. Louis, St Louis, Missouri 63130, USA. E-mail: pbiswas@wustl.edu*

† Electronic supplementary information (ESI) available. See DOI: 10.1039/c8ra05270k

supercapacitor. The flexible electrodes exhibit excellent electrochemical performance with capacitance of 445 F g^{-1} at 2 A g^{-1} and the long-term stability (retained 84.1% capacitance after 2500 charge/discharge cycles). The flexible solid-state supercapacitor fabricated using PEDOT:PSS/SnO_2/rGO/BNC as electrodes and poly(vinyl alcohol) (PVA)-H_2SO_4 coated BNC as separator showed excellent energy storage performance. Furthermore, the integrated device showed small capacitance decay over 2500 charge/discharge cycles.

2. Experimental section

2.1 Materials

Potassium stannate trihydrate (99.9% trace metals basis), urea, graphite flakes, potassium permanganate, hydrogen peroxide, hydrochloric acid, PEDOT:PSS (1.0 wt% in H_2O, high-conductivity grade), hypophosphorous acid (HPA, 50%), iodine (I_2), and poly(vinyl alcohol) (PVA, M_w 146000–186000, 99+% hydrolyzed) were purchased from Sigma-Aldrich.

2.2 Preparation of SnO_2 nanoparticles

0.12 g of urea was added into 20 ml mixture containing ethanol and water with a volume ratio of 3 : 5. 0.096 g of potassium stannate trihydrate was slowly added into this mixture with constant stirring. The mixture solution was transferred to a Teflon-lined stainless steel autoclave and heated in an oven at 190 °C for 24 h. The product was centrifuged and washed with nanopure water and ethanol several times and redispersed in nanopure water.

2.3 Preparation of PEDOT:PSS/SnO_2/rGO/BNC electrodes

GO was prepared using the procedure reported by Marcano *et al.*[33] *Gluconacetobacter hansenii* (ATCC®53582) was cultured in test tubes containing 16 ml of #1765 medium at 30 °C under shaking at 250 rpm. The #1765 medium is composed of 2% (w/v) glucose, 0.5% (w/v) yeast extract, 0.5% (w/v) peptone, 0.27% (w/v) disodium phosphate, and 0.5% (w/v) citric acid. Graphene oxide solution (5 ml of 0.3 wt%) was centrifuged and re-dispersed in #1765 medium and then centrifuged again to leave a wet mixture of GO and medium after decanting supernatant. SnO_2 nanoparticles were washed with #1765 medium, centrifuged and then re-dispersed in #1765 medium. Bacterial culture solution (incubated 3 days) and SnO_2 nanoparticles in #1765 medium were added to the GO/medium wet mixture to make it to a total of 15 ml (with GO concentration of 0.1 wt%, SnO_2 concentration of 0.5 mg ml^{-1}) and mixed thoroughly. The solution was transferred to a Petridish and incubated at room temperature for 7 days. The BNC film was harvested and washed in 0.1 M NaOH aqueous solution under boiling condition for 2 h then washed in nanopure water. The reduction of graphene oxide was performed according to the procedure reported by Pham *et al.*[34] The washed SnO_2/GO/BNC hydrogel was immersed in a 300 ml solution containing 100 g of HPA and 5 g of I_2 and heated at 85 °C for 12 h. Then the SnO_2/rGO/BNC was washed with nanopure water and dried. PEDOT:PSS was added on the SnO_2/rGO/BNC film and dried under the ambient condition to form PEDOT:PSS/SnO_2/rGO/BNC electrodes. The mass of the electrodes was measured using microbalance, and the mass of active materials loading is measured to be 0.57 mg cm^{-2}.

2.4 Preparation of flexible solid-state supercapacitor

Electrolyte was prepared by mixing 2 g of PVA and 2 g of H_2SO_4 in 20 ml of nanopure water and then heated at 85 °C until the solution became clear. After the PVA-H_2SO_4 electrolyte was cooled to room temperature, a piece of BNC film was immersed in it for 10 min. Then the PVA-H_2SO_4 coated BNC film was sandwiched between PEDOT:PSS/SnO_2/rGO/BNC electrodes and dried at room temperature overnight to form a flexible solid-state supercapacitor.

2.5 Characterization

SEM images were collected using FEI Nova NanoSEM 2300. AFM image was collected from Dimension 3000 (Bruker). Raman spectrum was collected from Renishaw inVia confocal Raman microscope. XPS spectrum was collected from VersaProbe II Scanning ESCA Microprobe. Electrical conductivity measurement is perform using the four-point probe station.[35]

2.6 Electrochemical measurement

All electrochemical measurements were performed using a CHI 760 bipotentiostat (CH Instruments, Austin, USA). Cyclic

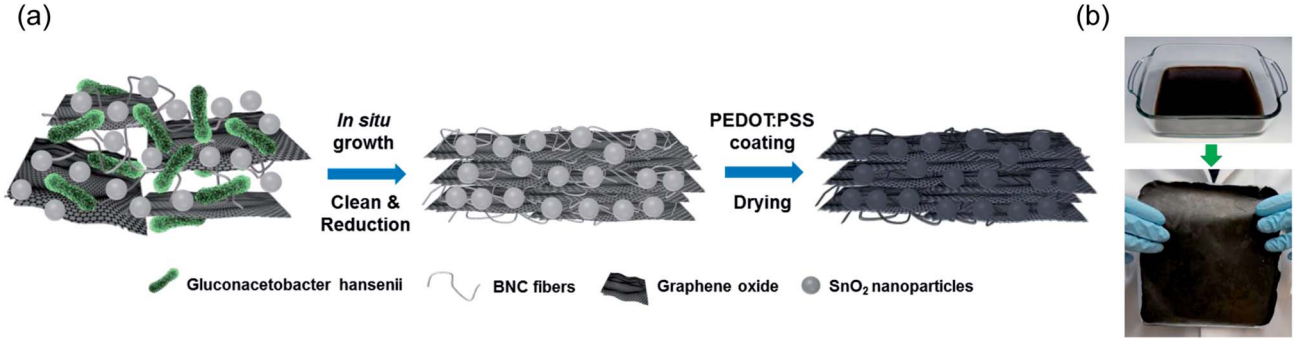

Fig. 1 (a) Schematic illustration showing the synthesis process of the PEDOT:PSS/SnO_2/rGO/BNC electrode for supercapacitor. (b) Photographs of the SnO_2/GO/BNC in hydrogel and dried states.

voltammetry was performed over a potential range of 0 to 1 V at scan rates of 5, 10, 25, 50, 100, 150, and 250 mV s^{-1}. Galvanostatic charge/discharge studies were carried out using a chronopotentiometry technique over a potential range of 0 to 1 V. Electrochemical studies were carried out using a three-electrode configuration for the single electrode and using a two-electrode configuration for the solid-state device. The three electrode configuration utilized the PEDOT:PSS/SnO_2/rGO/BNC composite as the working electrode, a platinum wire counter electrode, and an Ag/AgCl reference electrode, in a 1 M H_2SO_4 electrolyte solution.

3. Results and discussion

The fabrication of PEDOT:PSS/SnO_2/rGO/BNC electrode involves the culture of nanocellulose producing bacteria, *Gluconacetobacter hansenii*, in the presence of SnO_2 nanoparticles and GO flakes, followed by the reduction of GO and PEDOT:PSS coating (Fig. 1a). GO flakes were prepared according to a procedure reported previously with slight modification.[33] Atomic Force Microscope (AFM) image revealed the thickness of GO sheets to be around 1 nm (Fig. S1a in ESI†). Two characteristic bands at ~1591 and ~1352 cm^{-1} were observed in the

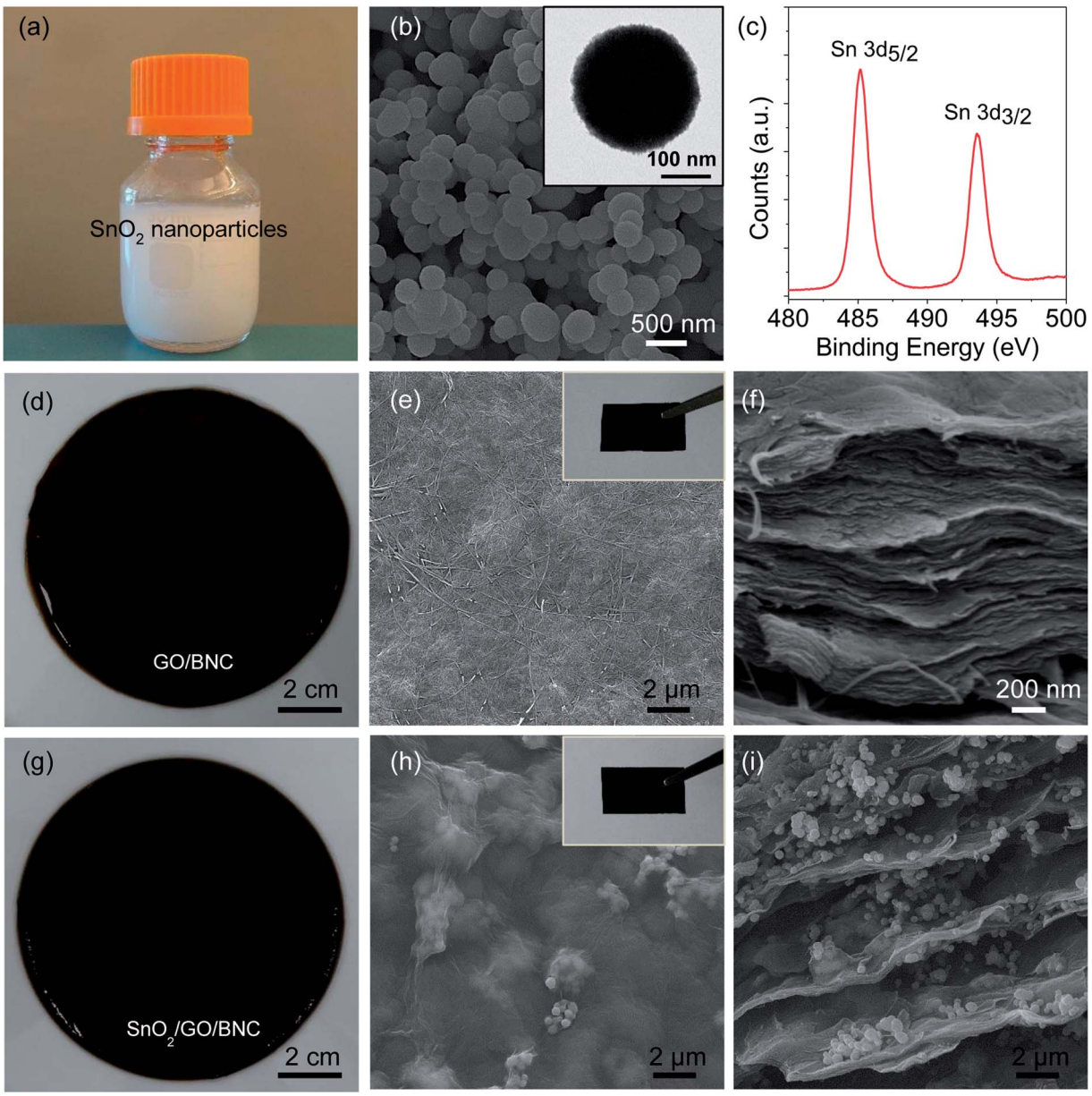

Fig. 2 (a) Photograph of the SnO_2 nanoparticles aqueous solution. (b) SEM image of the SnO_2 nanoparticles. Inset shows the TEM image of the SnO_2 nanoparticle. (c) X-ray photoelectron spectrum of the SnO_2 nanoparticles. (d) Photograph of the GO/BNC hydrogel. (e) SEM image of the top surface of the GO/BNC. Inset shows the photograph of the GO/BNC. (f) Cross-sectional SEM image of the GO/BNC. (g) Photograph of the SnO_2/GO/BNC hydrogel. (h) SEM image of the top surface of the SnO_2/GO/BNC. Inset shows the digital image of the SnO_2/GO/BNC film. (i) Cross-sectional SEM image of the SnO_2/GO/BNC.

Raman spectrum of GO, which correspond to the G-band and D-band, respectively (Fig. S1b in ESI†). SnO_2 nanoparticles were synthesized according to a procedure reported by Zhang *et al.* with slight modification (see Experimental section).[36] The SnO_2 growth solution is comprised of urea, potassium stannate trihydrate, and a mixture of ethanol and water. The mixture solution was placed in an autoclave reactor and heated in an oven at 190 °C for 24 hours. The aqueous solution of SnO_2 nanoparticles was found to be milky (Fig. 2a). Scanning and transmission electron microscope (SEM and TEM) images revealed the size of the SnO_2 nanoparticles to be 250–300 nm (Fig. 2b). X-ray photoelectron spectroscopy (XPS) was employed to investigate the surface chemical composition of the SnO_2 nanoparticles (Fig. 2c). Two strong peaks at around 485 eV and 494 eV can be attributed to Sn $3d_{5/2}$ and Sn $3d_{3/2}$, respectively, which confirm the formation of SnO_2 nanoparticles.[21,37,38] In a typical experiment for the preparation of SnO_2/GO/BNC film, GO flakes and SnO_2 nanoparticles were washed and re-dispersed in #1765 medium to form GO/medium and SnO_2/medium, separately (see Experimental section for details). A mixture solution containing a predetermined concentration of GO flakes and SnO_2 in the medium was homogeneously mixed with bacteria and set aside under static condition at room temperature for seven days for the formation of SnO_2/GO/BNC film in a semi-dry state (Fig. 1b top). The obtained SnO_2/GO/BNC film was washed in boiling NaOH solution and nanopure water. To reduce the GO, the washed SnO_2/GO/BNC film was immersed in a mixture of hypophosphorous acid (HPA) and iodine (I_2) according to previous report.[34] Then the SnO_2/rGO/BNC was washed with nanopure water and dried (Fig. 1b bottom). Fig. 2d and g show the semi-dry GO/BNC film without and with SnO_2 loading, respectively. SEM image of the GO/BNC film revealed an entangled network of BNC nanofibers and GO flakes embedded within the fiber network (Fig. 2e). The cross-sectional SEM image revealed the layered structure of GO/BNC film (Fig. 2f). SEM images of the SnO_2/GO/BNC film revealed the SnO_2 nanoparticles embedded within the GO/BNC layers (Fig. 2h and i). The electrical conductivity of SnO_2/rGO/BNC electrode exhibited a slight decrease with increasing the SnO_2 concentrations (Fig S2†) owing to the low conductivity nature of SnO_2. The conducting polymer, PEDOT:PSS, was added onto the SnO_2/rGO/BNC film, uniformly spread and dried under the ambient condition to form PEDOT:PSS/SnO_2/rGO/BNC electrodes.

Next, the electrochemical performance of the electrodes was investigated in a three-electrode configuration in 1 M H_2SO_4 electrolyte using cyclic voltammetry (CV) and galvanostatic charge–discharge (GCD) techniques. Presence of SnO_2 nanoparticles in the electrode results in a higher specific capacitance as evidenced by the CV curves. The specific capacitance (as represented by the integrated area in the CV curve) of PEDOT:PSS/SnO_2/rGO/BNC (402 F g^{-1}) is significantly higher than that of PEDOT:PSS/rGO/BNC (123 F g^{-1}) due to highly reversible faradaic redox processes associated with to SnO_2 (Fig. 3a). The fraction of pseudocapacitance in the total capacitance is calculated to be around 69%. The peak current of

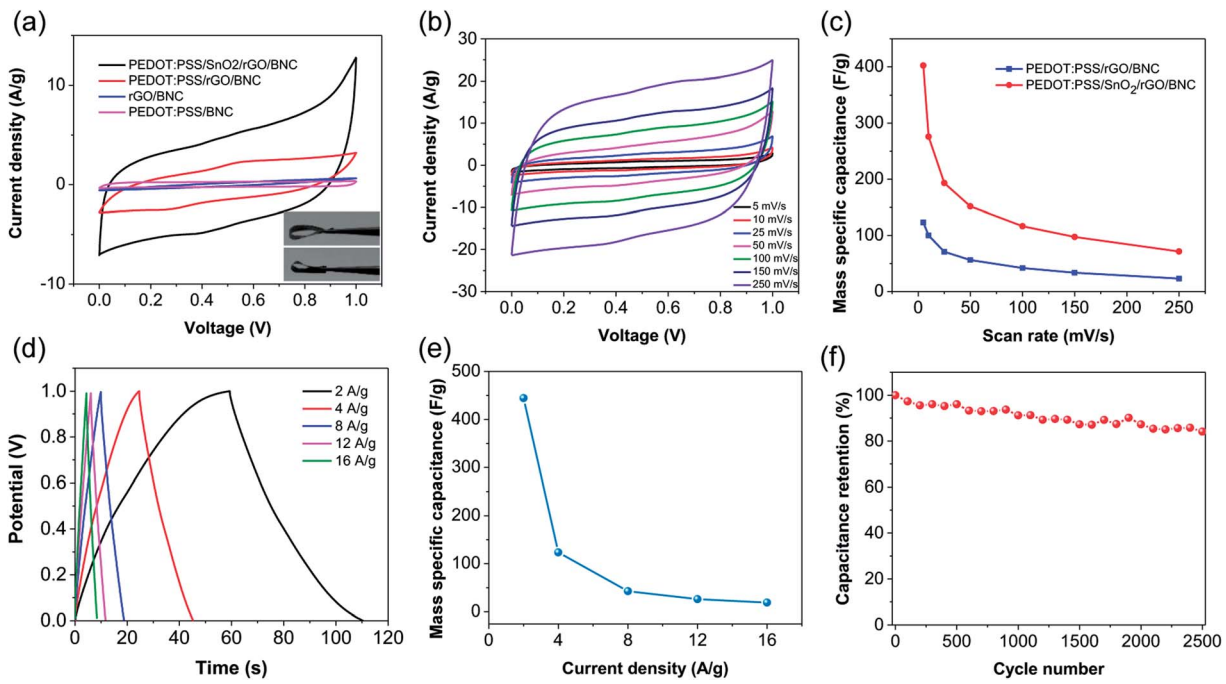

Fig. 3 Electrochemical performance of the PEDOT:PSS/rGO/BNC electrodes. (a) CV curves of the rGO/BNC, PEDOT:PSS/BNC, PEDOT:PSS/rGO/BNC and PEDOT:PSS/SnO_2/rGO/BNC electrodes at the scan rate of 50 mV s^{-1}. Insets show the digital images of the PEDOT:PSS/rGO/BNC electrodes without (top) and with (down) SnO_2 nanoparticles. (b) CV curves collected from various scan rates. (c) Mass specific capacitance with (red) and without (blue) SnO_2 nanoparticles at various scan rates. (d) Charge–discharge curves at various current densities. (e) Mass specific capacitance of the electrode with SnO_2 calculated from the charge–discharge curves at various current densities. (f) Cycling performance of the PEDOT:PSS/SnO_2/rGO/BNC electrode.

PEDOT:PSS/SnO_2/rGO/BNC electrodes exhibited an increase in the peak current upon scanning from 5 to 250 mV s^{-1} (Fig. 3b). The CV curves largely retain their rectangular shape, representative of an ideal capacitor, suggesting a fast charge transfer rate even at high scan rates. Specific capacitance ($C_{s,CV}$) of the electrodes decreased from 402 F g^{-1} to 72 F g^{-1} as the scan rate was increased from 5 to 250 mV s^{-1} (Fig. 3c). At the same scan rate, PEDOT:PSS/SnO_2/rGO/BNC electrodes exhibited higher specific capacitance compared to PEDOT:PSS/rGO/BNC. GCD curves collected at different current densities (2 to 16 A g^{-1}) exhibited typical triangular shape with symmetric charge–discharge profiles, further confirming the fast charge transfer rate (Fig. 3d). Additionally, only a small ohmic (IR) drop was observed at a scan rate of 16 A g^{-1}. The specific capacitance ($C_{s,GCD}$) of electrodes was found to decrease from 445 F g^{-1} to 19 F g^{-1} as the current density was increased from 2 to 16 A g^{-1} (Fig. 3e). The longevity and stability of the PEDOT:PSS/SnO_2/rGO/BNC electrodes was evaluated using GCD technique for 2500 cycles at a current density of 2 A g^{-1} (Fig. 3f). The electrode retains 84.1% of its initial capacitance over 2500 charge–discharge cycles, indicating this composite electrode is a promising candidate for supercapacitor devices.

The solid-state supercapacitor devices were prepared using two electrodes separated by a BNC film saturated with PVA-H_2SO_4 as electrolyte (Fig. 4a). Considering that the electrode fabrication approach is highly scalable, large electrodes and separator films can be easily synthesized and assembled into a flexible device (Fig. 4b right and middle respectively). The supercapacitor retains a quasi-rectangular shaped CV curves at sweep rates lower than 50 mV s^{-1} but exhibit deviation at high scan rates indicating a high charge-transfer resistance (Fig. 4c). GCD curves were obtained at various current densities from 0.5 to 4 A g^{-1} to probe the cycling performance and capacitance retention. The charge–discharge curves were found to be symmetric triangles with no signs of significant self-discharge, indicating a highly reversible charge–discharge process (Fig. 4d). Specific capacitance ($C_{s,GCD}$) of device showed a decrease from 603 to 55 F g^{-1} as the current density was

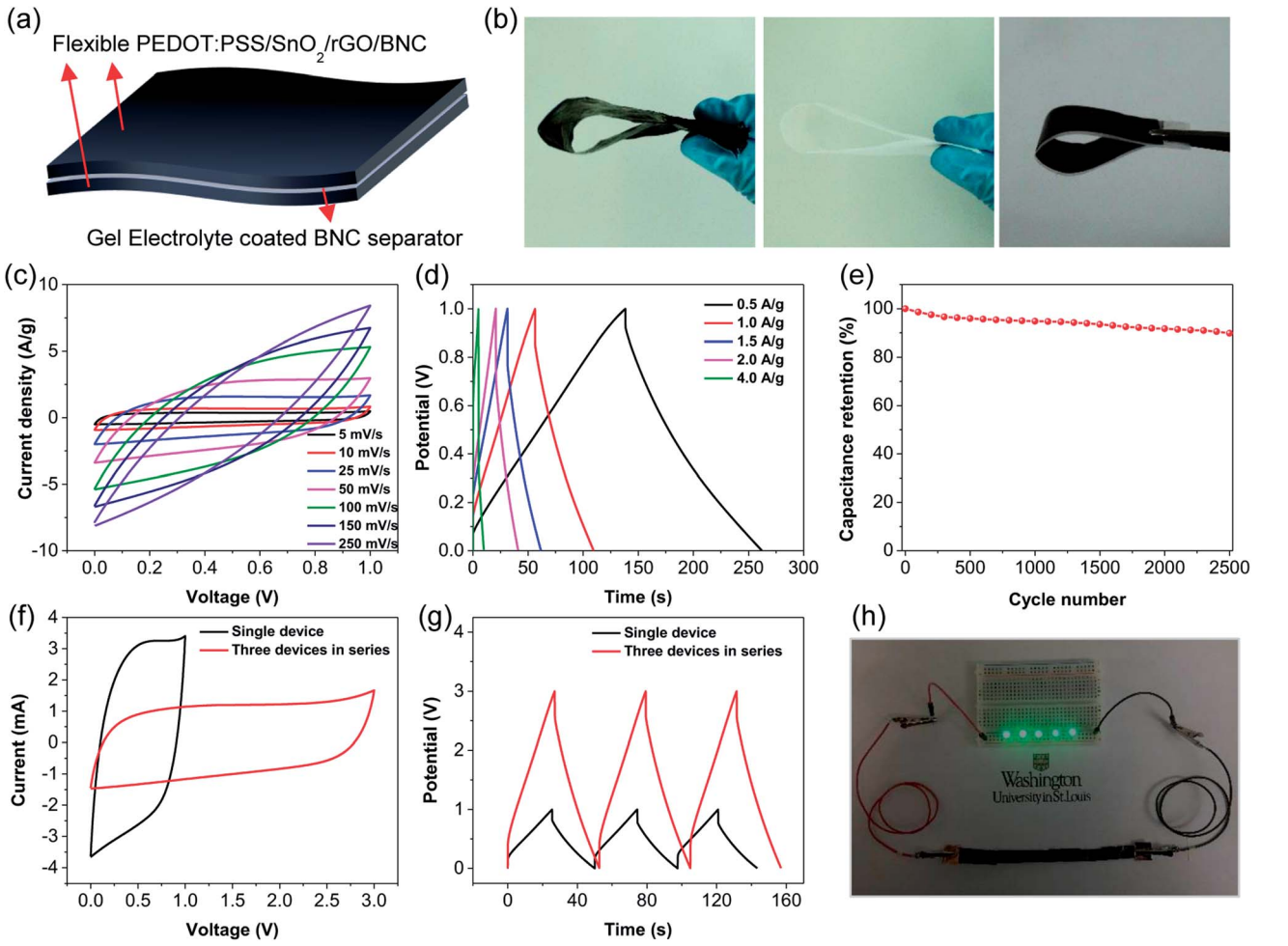

Fig. 4 (a) Schematic illustration of PEDOT:PSS/SnO_2/rGO/BNC electrodes based flexible solid-state supercapacitor. (b) Photograph of the electrode (left), BNC separator (middle), and flexible solid-state supercapacitor device (right). (c) CV curves of the supercapacitor at various scan rates. (d) Charge–discharge curves of the supercapacitor at various current densities. (e) Cycling performance of the PEDOT:PSS/SnO_2/rGO/BNC based supercapacitor. (f) CV curves of the supercapacitor at 50 mV s^{-1} and (g) charge–discharge curves at 2.0 mA of a single supercapacitor device (black) and three devices in series (red). (h) Photograph of five LEDs powered by the supercapacitors in series.

increased from 0.5 to 4 A g^{-1} (Fig. S3†). CV curves of the supercapacitor device under different bending angles reveals the excellent flexibility and stability (Fig. S4†). Cycling performance was studied to determine the capacitance retention of the supercapacitor device over 2500 cycles at a charge rate of 2 A g^{-1}. The device retained 89.8% capacitance after 2500 cycles demonstrating an excellent capacitance retention (Fig. 4e). Three devices were then connected in series to power a series of light emitting diodes. The CV curve of the three-device chain retains the rectangular shape even when charged to high voltage, indicating no large charge transfer resistances are added by connecting the devices in series (Fig. 4f). Similarly, GCD measurements of the three-devices in series show that the device chain can be charged in approximately the same amount of time as a single device, and retains the ideal symmetrical shape (Fig. 4g). Furthermore, the three-device chain of the flexible solid-state supercapacitor was charged and able to power a series of blue LEDs, demonstrating the potential application of this flexible energy storage device (Fig. 4h).

4. Conclusion

In conclusion, we have demonstrated a novel and facile method for the fabrication of PEDOT:PSS/SnO_2/rGO/BNC electrodes for the fabrication of flexible, lightweight, and solid-state hybrid supercapacitor. The energy storage performance of the electrodes exhibited a significant improvement with the incorporation of SnO_2 nanoparticles. The electrodes exhibit excellent electrochemical performance with specific capacitance of 445 F g^{-1} at the current density of 2 A g^{-1}. The longevity and stability of PEDOT:PSS/SnO_2/rGO/BNC electrodes was evaluated by obtaining GCD curves and 84.1% of its original capacitance was retained after 2500 cycles at a current density of 2 A g^{-1}. The materials and the fabrication process are scalable and cost-effective, which makes BNC-based supercapacitors promising candidates for flexible and wearable solid-state energy storage devices.

Conflicts of interest

There are no conflicts to declare.

Acknowledgements

This work was supported by Air Force Office of Scientific Research (AFOSR), award number: FA9550-15-1-0228. This work was performed in part at the Nano Research Facility (NRF), a member of the National Nanotechnology Infrastructure Network (NNIN). The authors thank Professor Julio M. D'Arcy in Department of Chemistry at Washington University for providing access to four-point probe station and thank Yang Lu for performing the experiment.

Notes and references

1 W. Liu, M.-S. Song, B. Kong and Y. Cui, Flexible and Stretchable Energy Storage: Recent Advances and Future Perspectives, *Adv. Mater.*, 2017, **29**, 1603436.
2 Z. Liu, Z.-S. Wu, S. Yang, R. Dong, X. Feng and K. Müllen, Ultraflexible In-Plane Micro-Supercapacitors by Direct Printing of Solution-Processable Electrochemically Exfoliated Graphene, *Adv. Mater.*, 2016, **28**, 2217–2222.
3 L. Wen, F. Li and H.-M. Cheng, Carbon Nanotubes and Graphene for Flexible Electrochemical Energy Storage: from Materials to Devices, *Adv. Mater.*, 2016, **28**, 4306–4337.
4 Q. Xue, J. Sun, Y. Huang, M. Zhu, Z. Pei, H. Li, Y. Wang, N. Li, H. Zhang and C. Zhi, Recent Progress on Flexible and Wearable Supercapacitors, *Small*, 2017, 1701827.
5 L. L. Zhang and X. S. Zhao, Carbon-based materials as supercapacitor electrodes, *Chem. Soc. Rev.*, 2009, **38**, 2520–2531.
6 G. Wang, L. Zhang and J. Zhang, A review of electrode materials for electrochemical supercapacitors, *Chem. Soc. Rev.*, 2012, **41**, 797–828.
7 L. Hu, J. W. Choi, Y. Yang, S. Jeong, F. La Mantia, L.-F. Cui and Y. Cui, Highly conductive paper for energy-storage devices, *Proc. Natl. Acad. Sci.*, 2009, **106**, 21490–21494.
8 K. Jost, C. R. Perez, J. K. McDonough, V. Presser, M. Heon, G. Dion and Y. Gogotsi, Carbon coated textiles for flexible energy storage, *Energy Environ. Sci.*, 2011, **4**, 5060–5067.
9 Y. Xu, Z. Lin, X. Huang, Y. Wang, Y. Huang and X. Duan, Functionalized Graphene Hydrogel-Based High-Performance Supercapacitors, *Adv. Mater.*, 2013, **25**, 5779–5784.
10 H. Wang, B. Zhu, W. Jiang, Y. Yang, W. R. Leow, H. Wang and X. Chen, A Mechanically and Electrically Self-Healing Supercapacitor, *Adv. Mater.*, 2014, **26**, 3638–3643.
11 Q. Wang, J. Yan and Z. Fan, Carbon materials for high volumetric performance supercapacitors: design, progress, challenges and opportunities, *Energy Environ. Sci.*, 2016, **9**, 729–762.
12 M. Sawangphruk, P. Srimuk, P. Chiochan, A. Krittayavathananon, S. Luanwuthi and J. Limtrakul, High-performance supercapacitor of manganese oxide/reduced graphene oxide nanocomposite coated on flexible carbon fiber paper, *Carbon*, 2013, **60**, 109–116.
13 M. Sawangphruk, M. Suksomboon, K. Kongsupornsak, J. Khuntilo, P. Srimuk, Y. Sanguansak, P. Klunbud, P. Suktha and P. Chiochan, High-performance supercapacitors based on silver nanoparticle–polyaniline–graphene nanocomposites coated on flexible carbon fiber paper, *J. Mater. Chem. A*, 2013, **1**, 9630–9636.
14 L. Yuan, X. Xiao, T. Ding, J. Zhong, X. Zhang, Y. Shen, B. Hu, Y. Huang, J. Zhou and Z. L. Wang, Paper-Based Supercapacitors for Self-Powered Nanosystems, *Angew. Chem., Int. Ed.*, 2012, **51**, 4934–4938.
15 C. Choi, H. J. Sim, G. M. Spinks, X. Lepró, R. H. Baughman and S. J. Kim, Elastomeric and Dynamic MnO_2/CNT Core–Shell Structure Coiled Yarn Supercapacitor, *Adv. Energy Mater.*, 2016, **6**, 1502119.
16 G. Yu, L. Hu, N. Liu, H. Wang, M. Vosgueritchian, Y. Yang, Y. Cui and Z. Bao, Enhancing the Supercapacitor Performance of Graphene/MnO_2 Nanostructured Electrodes by Conductive Wrapping, *Nano Lett.*, 2011, **11**, 4438–4442.

17 L. Huang, D. Chen, Y. Ding, S. Feng, Z. L. Wang and M. Liu, Nickel–Cobalt Hydroxide Nanosheets Coated on $NiCo_2O_4$ Nanowires Grown on Carbon Fiber Paper for High-Performance Pseudocapacitors, *Nano Lett.*, 2013, **13**, 3135–3139.

18 X. Cao, Y. Shi, W. Shi, G. Lu, X. Huang, Q. Yan, Q. Zhang and H. Zhang, Preparation of Novel 3D Graphene Networks for Supercapacitor Applications, *Small*, 2011, **7**, 3163–3168.

19 V. Augustyn, P. Simon and B. Dunn, Pseudocapacitive oxide materials for high-rate electrochemical energy storage, *Energy Environ. Sci.*, 2014, **7**, 1597–1614.

20 Y. Wang, Z. X. Huang, Y. Shi, J. I. Wong, M. Ding and H. Y. Yang, Designed hybrid nanostructure with catalytic effect: beyond the theoretical capacity of SnO_2 anode material for lithium ion batteries, *Sci. Rep.*, 2015, **5**, 9164.

21 Y.-X. Wang, Y.-G. Lim, M.-S. Park, S.-L. Chou, J. H. Kim, H.-K. Liu, S.-X. Dou and Y.-J. Kim, Ultrafine SnO_2 nanoparticle loading onto reduced graphene oxide as anodes for sodium-ion batteries with superior rate and cycling performances, *J. Mater. Chem. A*, 2014, **2**, 529–534.

22 P. Simon and Y. Gogotsi, Materials for electrochemical capacitors, *Nat. Mater.*, 2008, **7**, 845–854.

23 J. R. Miller and P. Simon, Electrochemical Capacitors for Energy Management, *Science*, 2008, **321**, 651–652.

24 Y. Ko, M. Kwon, W. K. Bae, B. Lee, S. W. Lee and J. Cho, Flexible supercapacitor electrodes based on real metal-like cellulose papers, *Nat. Commun.*, 2017, **8**, 536.

25 Z. Wang, P. Tammela, M. Strømme and L. Nyholm, Cellulose-based Supercapacitors: Material and Performance Considerations, *Adv. Energy Mater.*, 2017, **7**, 1700130.

26 Z. Gui, H. Zhu, E. Gillette, X. Han, G. W. Rubloff, L. Hu and S. B. Lee, Natural Cellulose Fiber as Substrate for Supercapacitor, *ACS Nano*, 2013, **7**, 6037–6046.

27 L. Hu and Y. Cui, Energy and environmental nanotechnology in conductive paper and textiles, *Energy Environ. Sci.*, 2012, **5**, 6423–6435.

28 L. Yuan, B. Yao, B. Hu, K. Huo, W. Chen and J. Zhou, Polypyrrole-coated paper for flexible solid-state energy storage, *Energy Environ. Sci.*, 2013, **6**, 470–476.

29 L. Liu, Z. Niu, L. Zhang, W. Zhou, X. Chen and S. Xie, Nanostructured Graphene Composite Papers for Highly Flexible and Foldable Supercapacitors, *Adv. Mater.*, 2014, **26**, 4855–4862.

30 A. Razaq, L. Nyholm, M. Sjödin, M. Strømme and A. Mihranyan, Paper-Based Energy-Storage Devices Comprising Carbon Fiber-Reinforced Polypyrrole-Cladophora Nanocellulose Composite Electrodes, *Adv. Energy Mater.*, 2012, **2**, 445–454.

31 C. Chen, Y. Zhang, Y. Li, J. Dai, J. Song, Y. Yao, Y. Gong, I. Kierzewski, J. Xie and L. Hu, All-wood, low tortuosity, aqueous, biodegradable supercapacitors with ultra-high capacitance, *Energy Environ. Sci.*, 2017, **10**, 538–545.

32 Q. Jiang, C. Kacica, T. Soundappan, K.-k. Liu, S. Tadepalli, P. Biswas and S. Singamaneni, An *in situ* grown bacterial nanocellulose/graphene oxide composite for flexible supercapacitors, *J. Mater. Chem. A*, 2017, **5**, 13976–13982.

33 D. C. Marcano, D. V. Kosynkin, J. M. Berlin, A. Sinitskii, Z. Sun, A. Slesarev, L. B. Alemany, W. Lu and J. M. Tour, Improved Synthesis of Graphene Oxide, *ACS Nano*, 2010, **4**, 4806–4814.

34 H. D. Pham, V. H. Pham, T. V. Cuong, T.-D. Nguyen-Phan, J. S. Chung, E. W. Shin and S. Kim, Synthesis of the chemically converted graphene xerogel with superior electrical conductivity, *Chem. Commun.*, 2011, **47**, 9672–9674.

35 Y. Lu, L. M. Santino, S. Acharya, H. Anandarajah and J. M. D'Arcy, Studying Electrical Conductivity Using a 3D Printed Four-Point Probe Station, *J. Chem. Educ.*, 2017, **94**, 950–955.

36 C. Zhang, H. B. Wu, C. Yuan, Z. Guo and X. W. Lou, Confining Sulfur in Double-Shelled Hollow Carbon Spheres for Lithium–Sulfur Batteries, *Angew. Chem., Int. Ed.*, 2012, **51**, 9592–9595.

37 R. Tian, Y. Zhang, Z. Chen, H. Duan, B. Xu, Y. Guo, H. Kang, H. Li and H. Liu, The effect of annealing on a 3D SnO_2/graphene foam as an advanced lithium-ion battery anode, *Sci. Rep.*, 2016, **6**, 19195.

38 W. Wang, Q. Hao, W. Lei, X. Xia and X. Wang, Graphene/SnO_2/polypyrrole ternary nanocomposites as supercapacitor electrode materials, *RSC Adv.*, 2012, **2**, 10268–10274.